Mechanism and Kinetics of Fullerene Association in Polystyrene Thin Film Mixtures

ARTICLE *in* MACROMOLECULES · MAY 2011

Impact Factor: 5.8 · DOI: 10.1021/ma2004458

2 AUTHORS:

Him Cheng Wong
Singapore University of Technology and Desi…
19 PUBLICATIONS **208** CITATIONS
SEE PROFILE

João T Cabral
Imperial College London
85 PUBLICATIONS **1,246** CITATIONS
SEE PROFILE

Macromolecules

ARTICLE

pubs.acs.org/Macromolecules

Mechanism and Kinetics of Fullerene Association in Polystyrene Thin Film Mixtures

Him Cheng Wong and João T. Cabral*

Department of Chemical Engineering, Imperial College London, London SW7 2AZ, U.K.

ABSTRACT: We study the mechanism and kinetics of fullerene C_{60} association in model homopolymer thin films upon isothermal annealing. Uniform polystyrene (PS) films loaded with 0−5% C_{60} mass fraction, on both sides of the miscibility threshold, are annealed and monitored over time. A transition from heterogeneous, sparse, nucleation to a percolated spinodal morphology is observed with increasing C_{60} loading and time. Fullerene association is followed by crystallization, which is quantified by Avrami kinetics in two dimensions. Key regimes of the process are identified as nucleation, percolation, saturation and coarsening stages, and defined in terms of the evolution of cluster average size $\langle r \rangle$, number density N_d, area fraction A_f, and dominant wavenumber q^*. The "spinodal clustering" process results in a percolated lateral morphology and undulating surface topography whose wavelength λ and amplitude δh can be tuned with temperature T, time t, film thickness h and polymer molecular mass M_w. These results provide insight into pattern formation in nanocomposites relevant to engineering functional materials, including organic photovoltaics and thin film coatings.

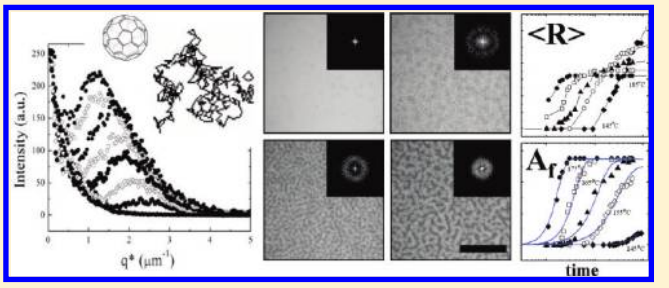

I. INTRODUCTION

Controlling the structure and stability of nanofillers in polymer matrices is key to the development of functional nanocomposites.[1] The miscibility and dispersion of polymer−nanoparticle mixtures is governed by a subtle balance of enthalpic and entropic contributions,[1−3] in addition to interfacial wetting in thin films,[4,5] all of which control the spatial arrangement at the nanoscale and thereby the macroscopic performance of the composite material. Increasing experimental and theoretical work demonstrate the great *potential* gains in mechanical,[6] gas transport,[7] and optoelectronic properties[8] of nanostructured composites. Current applications range from advanced coatings[4,9−11] to photovoltaics.[8,12]

Polymer and fullerene-derivative mixtures are indeed among the most promising polymer solar cell materials reported so far, in terms of efficiency and stability,[12] as well as relative low cost. Their power conversion is governed by the amount of donor/acceptor interface generated in bulk heterojunction device structures, which rely on the nanoscale phase separation within the thin (∼100 nm) photoactive layer.[13−17] Performance is largely determined by the composite morphology, including amorphous and crystalline (polymer and fullerene) domains, and depends critically on film preparation and post production thermal annealing.[18,19]

We have recently reported the spinodal association[20] of fullerene C_{60} in model polystyrene thin films, above the C_{60} miscibility threshold.[21] C_{60} in the nanocomposite films was found to nucleate within minutes of thermal annealing and percolate into well-defined spinodal-like pattern. The coarsening kinetics of the structure were quantified by the time-evolution of the dominant length scale λ^* and shown to follow a $\lambda^* \sim t^{\alpha}$, where t is time and α the coarsening exponent. α is $^1/_3$ for relatively thick films (170 nm) and gradually decreases to essentially 0 for ultrathin films,[20] as expected for the 2D phase separation in thin film confinement[22−24] which breaks the symmetry of the process. The $\alpha = {}^1/_3$ power law corresponds to evaporation−condensation and Brownian coalescence mechanisms in the bulk. The combination of film confinement and C_{60}−C_{60} affinity at this high fullerene loading leads to a collective nucleation process, named "spinodal clustering",[20] which is followed by crystallization. In this paper, we investigate the effect of concentration and temperature to elucidate the mechanism and kinetics of this polymer-fullerene association process.

II. EXPERIMENTAL SECTION

Uniform polystyrene−C_{60} nanocomposite thin films were prepared from dilute solution and spun-cast onto silicon wafer substrates. C_{60} was purchased from MER Corporation (99+% purity) and used as received; Polystyrene (PS) was obtained from BP Chemicals and purified by reprecipitation in 20-fold excess of methanol before use (M_w = 270 kg/mol, M_w/M_n = 2.4, R_g = 14 nm). PS and C_{60} fullerenes were separately dissolved in toluene (99.8+%, GLC, Fisher Scientific); the C_{60}-toluene solution was sonicated for 30 min and then added to the PS-toluene solution to obtain the required relative C_{60}-PS mass fraction. The mixture was further sonicated for 30 min, stirred, filtered (0.45 μm PTFE) and then spun-cast onto toluene-cleaned (100) silicon wafers (380 μm thick; ITME Poland) with a native (≈ 2 nm) oxide layer, characterized by X-ray reflectometry (PANalytical X'Pert PRO MPD).

Received: February 27, 2011
Revised: April 20, 2011
Published: May 10, 2011

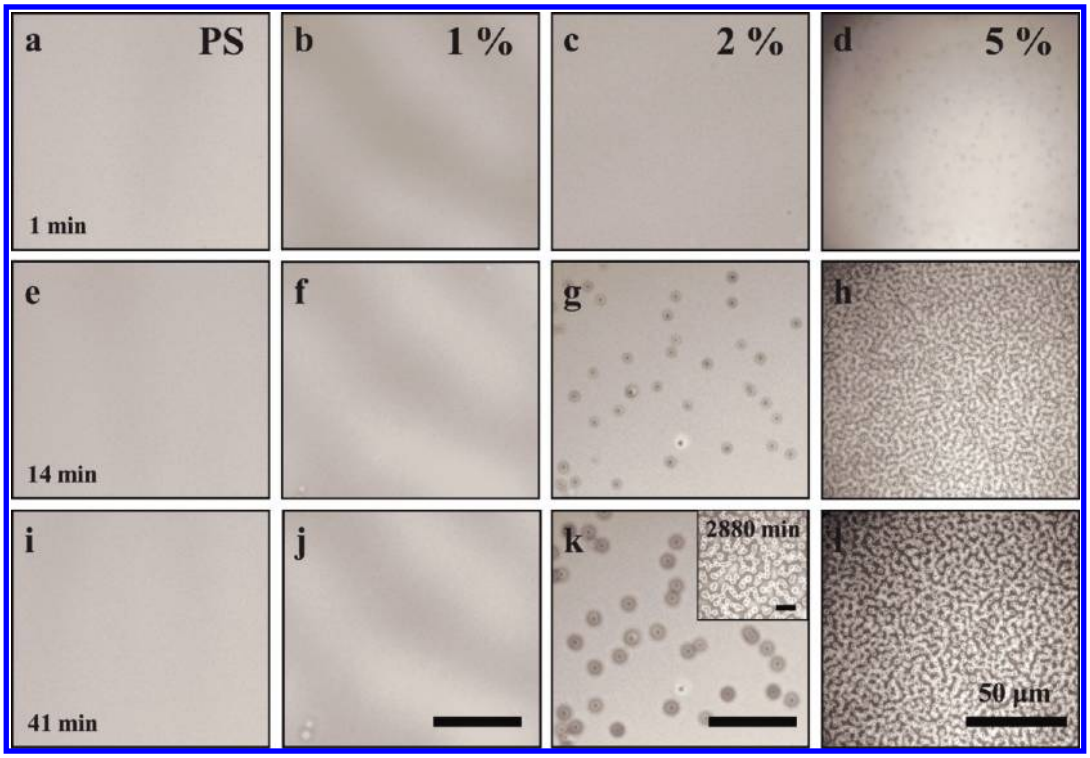

Figure 1. Optical micrographs of PS(270k) thin films (h = 150 nm) with different C_{60} loading, annealed isothermally at 175 °C for selected time intervals. A transition from stability to to sparse nucleation is visible between 1 and 2% mass fraction, and then to spinodal clustering at 5% C_{60}. The inset of panel k shows the 2% surface pattern after 2 days. Neat PS films remain uniform and (meta)stable for approximately 10 h. Scale bars are 50 μm.

Piranha-etched silicon substrates (Caution!) were also employed to probe possible surface energy effects.[25] A constant film thickness of approximately 150 ± 5 nm is used throughout this study, as measured by UV−vis interferometry (Filmetrics, F20−UV). The films were dried at room temperature for at least 24 h[26] and then isothermally annealed on a custom-made hot stage mounted on a reflection optical microscope (Olympus BX41M), equipped with an XY stage and CCD camera (AVT Marlin). Annealing temperatures within 100−185 °C and times of 0−2 days were investigated, with typical sampling intervals of 1 min. The surface topography of selected annealed films was characterized by atomic force microscopy (Innova, Bruker AXS) in tapping-mode, using super sharp TESP-SS tips. Wide angle X-ray scattering (WAXS) measurements on bulk PS−C_{60} sample were carried out with the multi purpose PANalytical (XPert Pro) diffractometer as a function of annealing times to study the development of crystallinity in the phase separated composite.

III. RESULTS AND DISCUSSION

The dependence of the PS−C_{60} thin film morphology on fullerene loading, upon isothermal annealing above the glass transition temperature T_g, is shown in Figure 1. Optical micrographs for 150 nm thick PS−C_{60} films annealed at 175 °C at representative times are selected for illustration. No sign of C_{60} association is observed at <2% C_{60} loading, while dense nucleation is observed at 2 wt % upon annealing. A "spinodal"-like structure develops within a few minutes in 5% C_{60} films, with well-defined dominant length scale and connectivity. Upon prolonged annealing over 48 h, the 2% mixture eventually percolates into an interconnected spinodal-like structure, which is qualitatively similar to 5% specimens, albeit less dense (thus with a larger characteristic length scale λ^*). Although a transition from nucleation to percolation is not apparent in the 5% C_{60} mixtures, the similarity between the final structures at 2 and 5% suggest a common association mechanism, starting with a nucleation and growth step. Subsequent experiments on the early stages of association at lower temperatures corroborate this hypothesis.

Various limits of miscibility and dispersibility of fullerenes in polymers have been reported.[21,27,28] The miscibility threshold of C_{60} in PS thin films agrees well with that measured in bulk PS, namely ≈1.5 wt %, established by calorimetry (DSC), dielectric spectroscopy (DS), small angle neutron scattering (SANS) and WAXS.[21,29] It is possible to disperse higher C_{60} loadings in PS via rapid precipitation (bulk) or spin-casting (thin films). However, we expect mixtures with C_{60} loading of 2% and above to demix upon annealing.

The undulations on the film surface (air interface) at 5% C_{60} loading do not correspond to spinodal dewetting,[30,31] as shown by the evolution of surface topography obtain by AFM. Further, neat PS films remain uniform within the experimental time window (Figure 1), and up to 10 h annealing, as expected for the (meta) stability of this relatively high PS M_w and film thickness.[31] In order to elucidate the underlying mechanism responsible for pattern formation on the nanocomposite surface, a combination of microscopy experiments and image analysis is employed.

A. Image Analysis. Quantitative image analysis of the thin film morphology and topography was carried out to characterize fullerene association and kinetics. Specifically, we probe the lateral (in-plane) morphology by a combination of optical microscopy (OM) and AFM, and the vertical topography (i.e., undulation amplitude) by AFM. Each pattern is thus quantified by its characteristic lateral length scale (λ^*) or wavenumber (q^*), average amplitude (δh), cluster average radius ($\langle r \rangle$), number density (N_d), and area fraction (A_f).

dx.doi.org/10.1021/ma2004458 |*Macromolecules* 2011, 44, 4530–4537

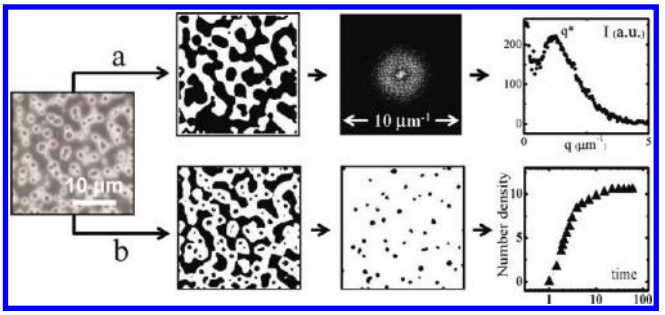

Figure 2. Image analysis procedure to quantify the time evolution of (a) the characteristic wavenumber (q^*) and (b) the number density (N_d), average radius ($\langle r \rangle$), and area fraction (A_f) of the clusters. A fast Fourier transform (FFT) and radial average of binary filtered image yields a structural dominant q^* and thus length scale $\lambda^* = 2\pi/q^*$. A filter of the bicontinuous envelope permits the determination of cluster statistics via procedure b. The procedure is illustrated with a PS(270K)-5 wt % C_{60} 150 nm thick film annealed at 175 °C for 61 min.

Figure 2 illustrates the image analysis procedure of an optical micrograph. Each pattern exhibits darker clusters corresponding to C_{60}-rich regions, surrounded by lighter connected domains, corresponding to undulations in film thickness. Each image is analyzed following two routes, to obtain (a) the characteristic length scale λ^* and (b) C_{60} cluster distribution statistics. Structure factors $S(q)$ of the film lateral bicontinuous morphology were obtained using ImageJ (NIH): images were thresholded and the cluster regions filled to create binary images that were then fast Fourier transformed (FFT) and radially averaged. The characteristic spatial frequency of the pattern was obtained by $\lambda^* = 2\pi/q^*$ where q^* is the wavenumber corresponding to the maximum intensity of $S(q)$. The coarsening kinetics of the in-plane structure $\lambda^*(t)$ were investigated as a function of isothermal annealing time (t). For comparison, neat PS films were investigated in the same experimental conditions. Route b yields cluster statistics, $\langle r \rangle$, N_d, and A_f, and was carried out using Vision Assistant (National Instruments 8); the same thresholding procedure was adopted, but now the connected "envelope" was removed. The characteristic cluster size $\langle r \rangle$ and polydispersity were obtained from the maximum and width of the cluster radius histogram. N_d is defined as the number of clusters per unit area and A_f their surface coverage normalized to image area. Measurement uncertainties were computed by varying image thresholding levels. For completion, the undulation average amplitude $\langle \delta h \rangle$ and maximum peak height of the surface topography were obtained from AFM data using the SPM Lab Analysis V7.00 software provided by Bruker AXS.

B. Cluster Characterization. The surface patterns are dominated by two features: dense clusters and surrounding interconnected domains. In order to ascertain the nature of the "clusters" formed, a combination of polarized microscopy and WAXS experiments were carried out. We have previously examined the bulk miscibility and thermal properties of PS(270K) and C_{60} with DSC, DS, SANS, and WAXS[21,29] to establish a threshold of ≈1.5% C_{60}, below which C_{60} remains dispersed even after prolonged annealing. It is therefore likely that the clusters observed are C_{60} rich, or pure C_{60}, domains. The area fraction obtained by image analysis tends asymptotically to 5% with annealing time, suggesting the latter, although an exact determination would require volume (3D) scanning.

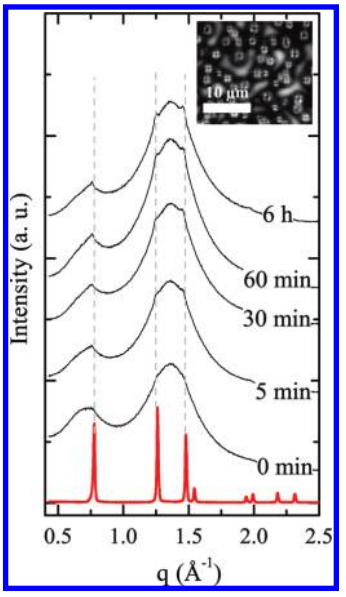

Figure 3. WAXS spectra for 5 wt % C_{60}-PS *bulk* mixtures as a function of annealing time at 180 °C. At 5 wt % C_{60} loading, the system is initially dispersed but, upon annealing, develops C_{60} crystalline peaks that match the WAXS spectrum of neat C_{60}, indicating fullerene crystallization upon agglomeration. Similar evidence of C_{60} crystallinity is also observed in the nanocomposite thin film (inset: 180 °C and 60 min) under cross-polarized microscopy. The WAXS data are shifted vertically for clarity.

WAXS experiments on PS−C_{60} mixtures of various loadings, acquired as a function of annealing time, help to clarify the cluster formation. The measurements are carried out on *bulk* specimens as nanocomposite thin films provide poor signal-to-noise ratios. Figure 3 shows that PS(270K)-5 wt % C_{60} annealed at 180 °C develops crystalline peaks that correspond to the crystallization of neat C_{60} at q = 0.77, 1.26, and 1.48 Å^{-1} within a few (2−5) min of annealing. This time scale agrees well with the onset of spinodal clustering in thin films. The inset of Figure 3 shows that C_{60} crystallites appear under cross-polarized microscopy, visible as Maltese crosses, in annealed nanocomposite films toward the later stages of annealing (shown here for 180 °C and 60 min). Prior to annealing, (fresh) nanocomposites only display C_{60} peaks if above the dispersibility threshold of ≈5%C_{60}. These experiments indicate that the "clusters" result from the phase separation of PS−C_{60} and ensuing crystallization of C_{60} within the polymer matrix.

C. Surface Topography. AFM scans of annealed nanocomposites characterize the development of the topography and provide additional height information. As mentioned earlier, an undulating bicontinuous morphology at the air interface could suggest spinodal dewetting. This has been reported in ultrathin polymers, including polystyrene films of $h \sim 5$ nm.[30,31] The early stages are well described by linearized capillary wave instability models, whereby thermally induced thickness fluctuations become unstable and grow exponentially with time, with dominant time-independent wavenumber $q^* = (3/2)^{1/2}(a/h^2)$ where a^2 is a surface interaction parameter (inversely dependent on viscosity η).[32] The initial wavelength λ of the structure is expected to follow $\lambda_0^* \sim h^2$, where h is film thickness. In the present case, however, the films do not actually dewet the substrate within experimental time scales (up to 48 h) and the film thicknesses (∼100 nm)

dx.doi.org/10.1021/ma2004458 |*Macromolecules* 2011, 44, 4530–4537

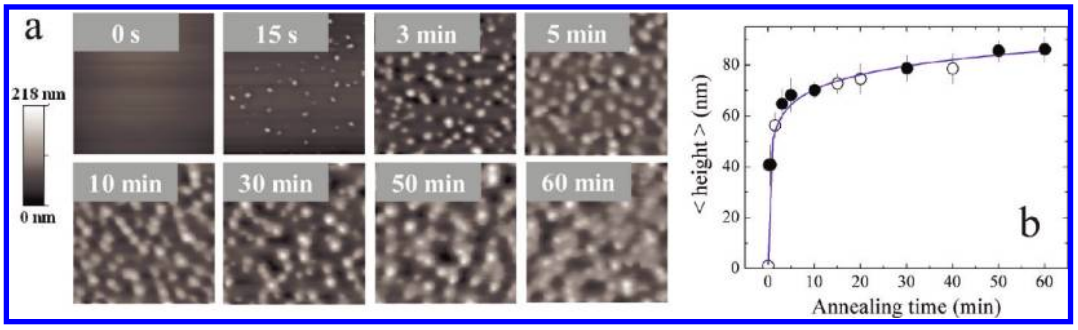

Figure 4. (a) AFM topography of PS(270K)-5 wt % C_{60} 150 nm film annealed at 175 °C for representative times. All images are 20 μm × 20 μm. (b) Average height of the surface topography as a function of annealing time. The solid line is a guide to the eye ($\langle h \rangle = \ln(t^k) + C$).

are much larger than expected for spinodal dewetting. Further, neat PS films under the same conditions remain uniform for approximately 12 h before slowly dewetting via nucleation of holes. By contrast, the nanocomposite surface topography develops with a few minutes (1−10 min) depending on annealing temperature.

In fact, C_{60} fullerenes[4,33,34] (and other nanoadditives)[9,34,35] have been found to actually suppress the dewetting of thin polymer films, including low M_w PS, providing an effective route to stabilizing thin polymer coatings. The underlying mechanism appears to involve the nanoparticle segregation to the substrate interface and this stratification then screens surface interactions and increases the interfacial viscosity, thereby pinning the contact lines of nucleating holes.[4] We have recently shown[20] that this fullerene association process depends on the polymer M_w and environmental conditions, and mapped the transition from uniform films to spinodal clustering. In the present case, we find no evidence of significant fullerene layering by neutron reflectivity.

Figure 4 shows AFM data and corresponding pattern average amplitude for a PS(270K)-5%C_{60} film of 150 nm thickness annealed at 175 °C. Clearly the film does not dewet the surface and, further, the amplitude growth (Figure 4b) can be well approximated by a logarithmic time dependence − in contrast with the exponential growth expected for spinodal dewetting. An Avrami fit ($\delta h \propto 1 - \exp(-Kt^n)$) is also compatible with the data and is discussed below. Selective dissolution of PS in the sample using tetrahydrofuran (THF) reveals that the micrometer-sized C_{60} aggregates (insoluble in THF) are anchored on the substrate, and retain the spinodal coordination. The combination of AFM scans on annealed and selectively dissolved films indicates that the morphology is composed on C_{60} aggregates covered by a PS top layer, resulting in an undulating surface topography that develops with time, with peak maximum amplitudes reaching between 200 and 300 nm after annealing at 175 °C for 60 min. This process is reminiscent of the 2D phase separation of polymer blends,[22−24] which results in surface buckling attributed to spatial surface tension variations accompanying demixing.

A recent study of film stability of PS−CdSe films onto silicon substrates seeded with sparsely distributed 120 nm SiO_2 particles[36] reports surface undulations, for films thinner that the large particle size, and overall film stability due to CdSe surface attraction. The final state of this self-assembly process exhibits interesting similarities with the current work, as it results in undulating yet stable films, with a coexistence of large particles (or clusters) and nanoparticles. However, the mechanisms differ in that the current work involves the association of a single type of nanoadditive, C_{60} fullerenes, and initiates from an otherwise uniform, flat thin film.

D. Coarsening Dynamics. Optical micrographs shown in Figure 5 show the coarsening of the lateral morphology during spinodal clustering for a representative 150 nm thick PS(270K)-5 wt % C_{60} film isothermally annealed at 175 °C. The films were inspected to be uniform and cluster free before annealing, as shown in Figure 5a. Within the first few minutes of annealing, the C_{60} fullerenes start to nucleate and both the size and number of nuclei increase until the system reaches a "saturation" stage. With further annealing, the spinodal-like in-plane structure coarsens with a $q^* \propto t^{-\alpha}$ relation. The coarsening exponent α is thickness dependent[20] and thinner films generally reduce the coarsening exponent α due to 2D confinement. After coarsening for nearly 2 orders of magnitude in time, the lateral structure eventually pins. Pinning has also been reported in 2D phase separation in thin films.[25] The image insets are the 2D fast Fourier transforms (FFT) of the optical micrographs. The structure factors at selected time intervals, obtained by radially averaging the FFTs, are summarized in Figure 6. The inset compiles the time evolution of q^* as a function of time for this sample. For this thickness and C_{60} loading, $\alpha \approx {}^1/_4$. The dependence of α on h has been reported previously[20] and agrees well with the current measurements.

E. Cluster Formation and Growth. In order to obtain a mechanistic understanding of fullerene association and pattern formation in polystyrene films, we quantify the key stages of the process in terms of the evolution of the average radius $\langle r \rangle$, cluster number density N_d, and area fraction A_f with time, in addition to the structure periodicity q^* reported above. Because of relatively fast clustering kinetics at high temperatures, the parameters were studied as a function of annealing temperature and time, as illustrated in Figure 7. At constant time (shown here for 60 min), the morphology ranges from sparse nucleation to spinodal-like percolation, as temperature increases from 145 to 175 °C.

We first consider the PS-5%C_{60} nanocomposite 150 nm film, annealed isothermally at 175 °C and reported in Figures 5 and 6. The time evolution of the cluster average radius $\langle r \rangle$, number density N_d, area fraction A_f, and dominant q^* are shown in Figure 8, parts a−d. For clarity, the process is divided in stages I−IV, according to distinct growth regimes. The process starts with the (I) *nucleation stage*, characterized by the appearance of clusters that grow in size, number and area fraction, but which lack interparticle correlations. The (II) *percolation stage* begins when a structural peak becomes visible in the radially averaged FFT, with characteristic maximum q^*. When the number of clusters (N_d) reaches its maximum, the pattern enters a (III) *saturation stage*.

dx.doi.org/10.1021/ma2004458 |*Macromolecules* 2011, 44, 4530–4537

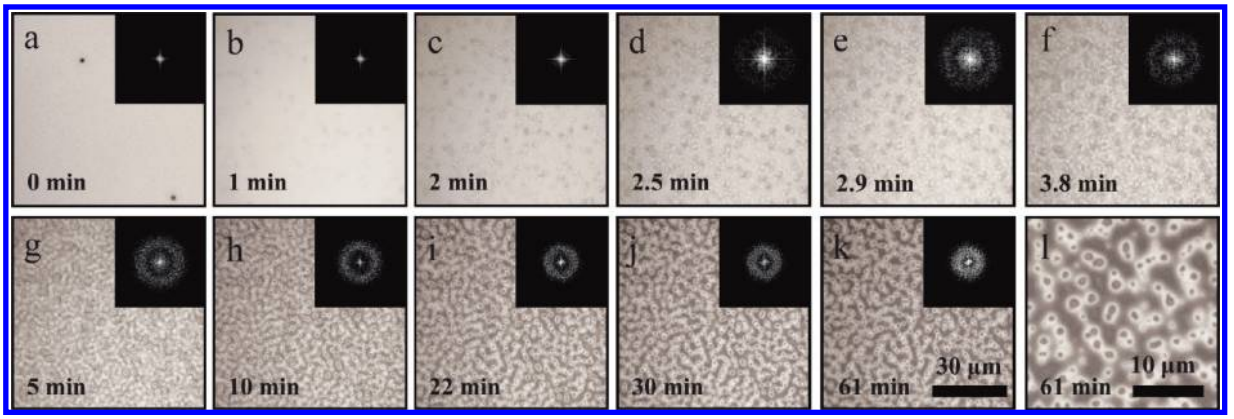

Figure 5. Coarsening morphology of spinodal clustering of a representative PS(270K)-5 wt % C_{60} thin film (h = 150 nm) annealed at 175 °C. Inset show the fast Fourier transforms (FFT) of the optical micrograph images (via route a). Panel l is a higher magnification of panel k, depicting the fullerene clusters and surrounding spinodal-like morphology.

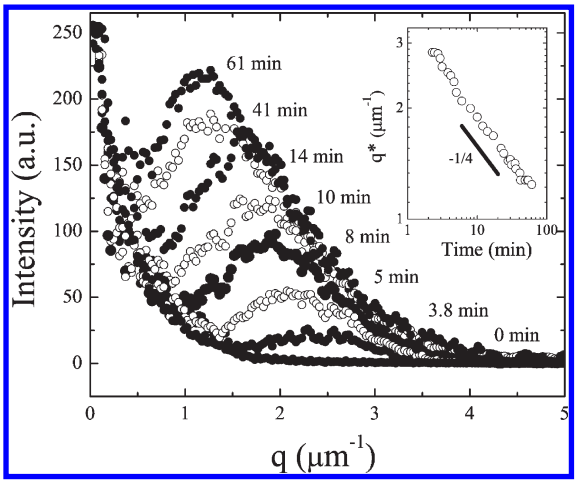

Figure 6. Evolution of the structure factor of PS(270K)-5 wt % C_{60} annealed at 175 °C, obtained by FFT and radial average of insets in Figure 5. The inset shows the time-dependence of the dominant wavenumber which scales as $q^* \propto t^{-1/4}$.

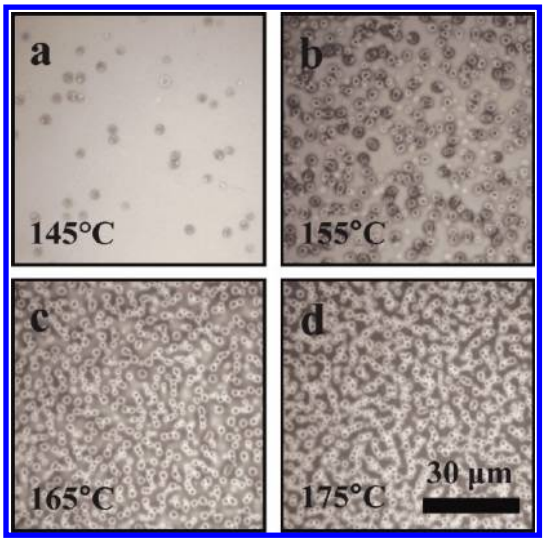

Figure 7. Surface morphology of a 150 nm PS(270K)-5 wt % film isothermally annealed at selected temperatures (a) 145 °C, (b) 155 °C, (c) 165 °C, and (d) 175 °C after 60 min.

Finally, a (IV) *coarsening stage* is reached when the size $\langle r \rangle$ and area fraction A_f of clusters also reach a maximum, yet coarsening of the film morphology continues. A_f reaches 5.5 ± 0.8% for PS-5% C_{60}, in agreement with our previous work.[20] At this temperature (175 °C), the transition between the regimes happens within 2.2 min (I−II), 4 min (II−III) and 10 min (III−IV).

The association process remains qualitatively similar to varying annealing temperatures, with an expected shift of time scales, clearly shown in Figure 8, parts e−h. However, there are significant quantitative changes worth noting. At the lowest temperature reported (145 °C), the association kinetics are considerably slower and there is now an induction period of approximately 10 min, during which no nuclei are observable using optical microscopy. Separately, the average cluster radius $\langle r \rangle$ depends on the annealing temperature and larger clusters are ultimately obtained at lower annealing temperatures. A crossover in radii occurs for the various annealing temperatures as a function of time. Inspection of the micrographs and population statistics indicates that this is caused by faster nucleation rates at higher temperatures, resulting in more clusters or smaller size. Cluster growth proceeds, consuming the "excess" C_{60} fullerenes in the matrix, until the area fraction over prolonged annealing converges to ≈5%. At higher temperatures, faster nucleation leads to increased monodispersity (inset of Figure 8e) while the coexistence of nucleation and growth at lower temperatures is responsible for a wide cluster size distribution.

The cluster volume fraction V_f can be geometrically estimated by a product of A_f and film thickness h and, since the clusters are noncylindrical, suitable approximations include a cone or a (hemi) oblate spheroid. For instance, a conical approximation yields $V_f \approx$ 1.8%, and thus ≈3% C_{60} mass fraction (slightly larger for hemispheroids). We have previously estimated a 1.5% miscibility limit for C_{60} in PS[21,29] and could thus expect an "excess" mass fraction of 3.5% which agrees reasonable well with observations. However, uncertainties in these geometrical consideration are large and we therefore restrict the discussion to the directly observable area fraction A_f.

Figure 8h indicates that the scaling power law remains $q^* \propto t^{-1/4}$ regardless of annealing temperature. The prefactor differs, of course, as the matrix viscosity and interfacial tension changes

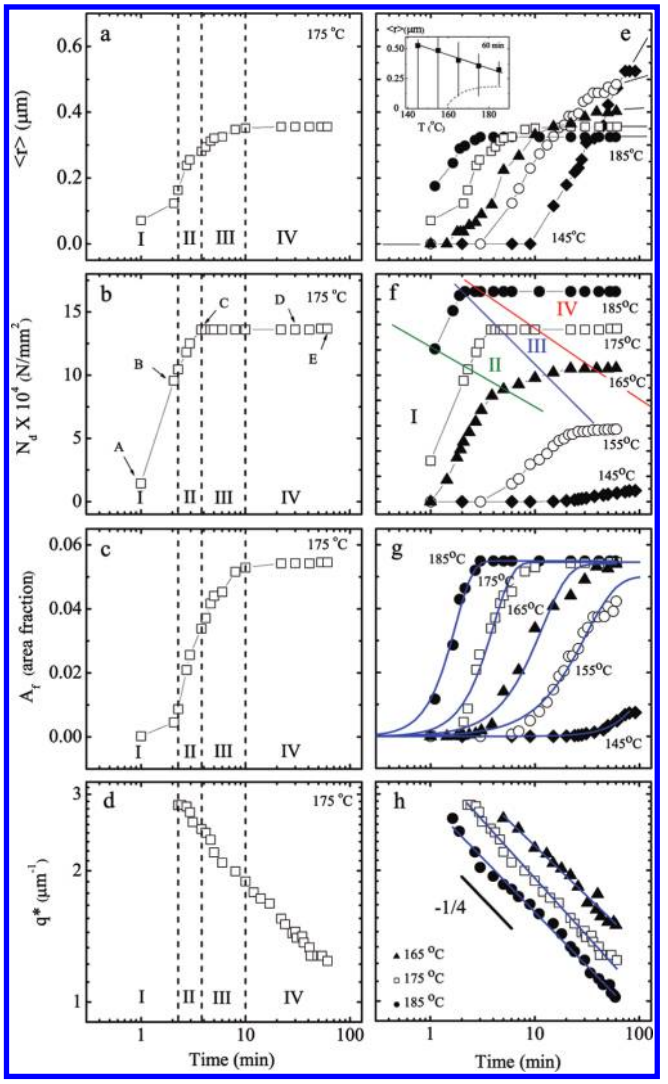

Figure 8. Time-dependence of the average radius $\langle r \rangle$, cluster number density N_d, cluster area fraction A_f, and characteristic wavenumber q^* for nanocomposite thin films PS-5% C_{60} with h = 150 nm. The left column (a–d) shows results for 175 °C annealing. I, II, III and IV denotes the nucleation, percolation, saturation and coarsening regimes (see text). The corresponding images for time points A to E are shown in Figure 5, parts b, c, f, j, and k, respectively. The right column (e–h) summarizes results for films annealed at various temperatures ranging from 145 to 185 °C. Red ticks denotes the onset time of nucleation regime before which the film is uniform and cluster-free. Green ticks show the onset for percolation regime while blue and purple ticks indicate the start of cluster saturation and structure coarsening. The inset of panel e shows the dependence of the cluster size distribution with annealing temperature, at constant time 60 min. Solid lines in panel g correspond to Avrami fits. A single exponent of $\alpha = {}^1/_4$ describes coarsening at all temperatures for constant thickness h = 150 nm.

with temperature.[37] The dependence of the scaling exponent with function of film thickness, at constant temperature, has been reported previously[20] to vary from ${}^1/_3 \rightarrow 0$, with decreasing thickness. This new result indicates that the exponent depends on film thickness, which in turn sets the C_{60} diffusion geometry, but not on temperature.

F. Avrami Kinetics. Figure 3 indicates that crystallization ensues fullerene agglomeration in the polymer matrix and

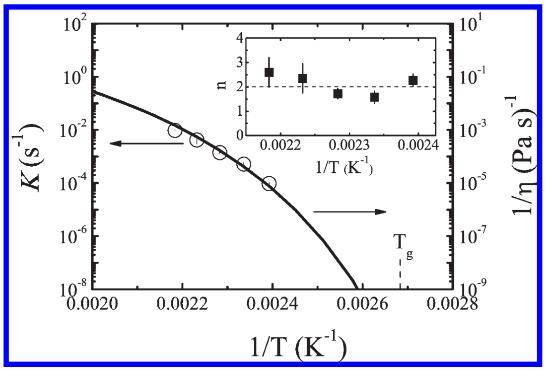

Figure 9. Temperature dependence of the Avrami kinetic parameter K (s^{-1}), describing fullerene association, overlaid onto the inverse viscosity η^{-1} of the polystyrene matrix computed by the WLF relation (see text). The inset depicts the Avrami exponent found to be $n \approx 2$.

suggests a quantitative analysis following Avrami kinetics:[38−40]

$$A_f = 1 - \exp((-Kt)^n) \quad (1)$$

where A_f is the crystallized area fraction, scaled to the maximum value, K is the kinetic constant and n is the Avrami exponent. We adopt a form of the Avrami relation that provides the correct physical dimensions[41] for the rate constant K in s^{-1}. As mentioned above, we estimate the crystalline volume fraction V_f by modeling the cluster peaks by a cone geometry. The relationship describes the crystallized area fraction A_f reasonably well, as shown by the solid lines in Figure 8g. The rate constant is found to be highly temperature dependent, ranging from 10^{-2} to 10^{-4} s^{-1} over a ΔT = 40 °C interval, and is plotted in Figure 9. The viscosity η of the PS matrix is overlaid on the graph for comparison, calculated according to the Williams–Landel–Ferry relation

$$\log\left(\frac{\eta(T)}{\eta(T_g)}\right) = \frac{-C_1(T - T_g)}{C_2 + (T - T_g)} \quad (2)$$

with PS constants C_1 = 14.6, C_2 = 50.4, and T_g = 100 °C.[42,43] K exhibits remarkable agreement with η^{-1} suggesting that, above the miscibility threshold, C_{60} association is largely mediated by the polymer matrix, as expected from the Stokes–Einstein relation $D = k_BT/6\pi\eta r$ where r is the particle radius. The results apparently contrast earlier observations of anomalous diffusion,[6,44] but can be reconciled by the fact that, at 5% loading (above the miscibility threshold), fullerenes associate during isothermal annealing into larger particles, eventually forming micrometer-sized clusters. The Avrami fits suggest an exponent $n \simeq 2$, as shown in the inset of Figure 9, which is expected for "circular" growth. This result can be understood given the large cluster diameter (reaching ≈1000 nm) and the smaller film thickness (150 nm), which corresponds to a 2D condition $h \ll d$.

Wang et al.[17] have recently reported on the crystallization of P3HT in solution cast P3HT:PCBM mixtures, a well-known organic photovoltaic composite, using grazing incidence X-ray scattering and ellipsometry. This bulk (3D) study revealed an Avrami exponent $n \approx 1.8$, which was associated with heterogeneous nucleation from aggregates or impurities. In the present case, PS is fully amorphous and thus only C_{60} crystallization is observed. Further work is underway to extend this approach to cocrystallizing composites.

dx.doi.org/10.1021/ma2004458 |*Macromolecules* 2011, 44, 4530–4537

IV. CONCLUSIONS

Thin films of PS−C_{60} above the miscibility threshold are shown to develop well-defined surface patterns, upon isothermal annealing above T_g. The pattern formation ranges from sparse nucleation to a coordinated spinodal-like morphology. The process starts with the polymer−fullerene phase separation, followed by C_{60} association and subsequent crystallization. Thin film confinement breaks the symmetry of the process and results in the undulation of the film surface, whereby the polymer covers the C_{60} clusters. The surface undulations are likely to be caused by a spatial modulation of surface tension. Selective dissolution of the polymer by selective solvent THF reveals that the micrometer-sized C_{60} aggregates are anchored on the substrate and retain the visible air interface pattern. The process is reminiscent of the 2D binary phase separation in polymer thin films.[22−24] At sufficiently high C_{60} loading (∼5%) and/or long annealing times, a distinctive spinodal-like structure develops with precisely controlled periodicity λ^* and height amplitude δh. Experiments on the early stages of the process at low temperatures show that the patterns stem from the heterogeneous nucleation of C_{60} rather than from spinodal decomposition (or dewetting). The process has been shown to depend on M_w.[20] Film uniformity and (meta)stability *can* be obtained for low M_w PS matrices,[4,20,33] under appropriate environmental conditions.[45] We also find the process to be robust to various substrate surface energy, including Piranha cleaning.[25]

Fullerene crystallization is adequately described by Avrami kinetics in 2D and great control can be exerted setting in the characteristic size, density and coordination of the C_{60} clusters. Diffusion of nanoparticles in thin films is expected to be faster than in bulk[44] and very anisotropic,[46] ie. considerably faster on the plane of the film than orthogonally, due to significant lubrication forces in a confined geometry. The crystallization rate K appears to follow the temperature dependence of the viscosity of *PS*, suggesting simple Stokes−Einstein diffusion through the polymer matrix.

A comparison between the C_{60} growth kinetics in the bulk, obtained by SANS,[21,47] and in present thin films suggests that C_{60} agglomeration is faster and more sensitive to temperature under confinement, but obeys a similar asymptotic trend. The aggregation temperature threshold T_c has been estimated at 160 °C in the bulk[21,47] and decreases to approximately 140 °C in 150 nm films, within the same experimental time scales of 1 day. The slightly lower T_c observed in thin films may be associated with increased mobility and T_g depression expected for supported PS films.[48]

The pattern periodicities λ^* and cluster sizes $\langle r \rangle$ obtained for this PS−C_{60} system are of the order of 1 μm and 100s nm, respectively and thus still far from the required 10−30 nm length scale in photovoltaics[8,12−17] but relevant to other coating applications, including for controlled wetting or optical properties. Smaller length scales are accessible by increasing the quench depth, which further increases the nucleation rate, as shown in Figure 8. However, deep quenches in this system are limited by the depolymerization of PS above ≈220 °C. This model system provides nevertheless clear strategies for the quantitative control of pattern formation in polymer−nanoparticle mixtures, relevant to structured composites, coatings and photovoltaics. Engineering the component miscibility and interaction parameters $\chi(T)$, which govern the driving force for phase separation, as well as the mobility of the species, should permit flexible tuning of association length and time scales for numerous nanocomposite applications.

AUTHOR INFORMATION

Corresponding Author
*E-mail: j.cabral@imperial.ac.uk.

ACKNOWLEDGMENT

The authors thank EPSRC for funding and Imperial College London for a studentship for HCW. We thank Jack F. Douglas, Anthony Higgins, Alamgir Karim, and David G. Bucknall for numerous helpful discussions.

REFERENCES

(1) Balazs, A. C.; Emrick, T.; Russell., T. P. *Science* **2006**, *314*, 1107.
(2) McGarrity, E. S.; Frischknecht, A. L.; Frink, L. J. D.; Mackay., M. E. *Phys. Rev. Lett.* **2007**, *99*, 238302.
(3) Akcora, P.; Liu, H.; Kumar, S. K.; Moll, J.; Li, Y.; Benicewicz, B. C.; Schadler, L. S.; Acehan, D.; Panagiotopoulos, A. Z.; Pryamitsyn, V.; Ganesan, V.; Ilavsky, J.; Thiyagarajan, P.; Colby, R. H.; Douglas., J. F. *Nat. Mater.* **2009**, *8*, 354.
(4) Barnes, K. A.; Karim, A.; Douglas, J. F.; Nakatani, A. I.; Gruell, H.; Amis., E. J. *Macromolecules* **2000**, *33*, 4177.
(5) Krishnan, R. S.; Mackay, M. E.; Hawker, C. J.; VanHorn., B. *Langmuir* **2005**, *21*, 5770.
(6) Mackay, M. E.; Dao, T. T.; Tuteja, A.; Ho, D. L.; Van Horn, B.; Kim, H. C.; Hawker., C. J. *Nat. Mater.* **2003**, *2*, 762.
(7) Merkel, T. C.; Freeman, B. D.; Spontak, R. J.; He, Z.; Pinnau, I.; Meakin, P.; Hill., A. J. *Science* **2002**, *296*, 519.
(8) Sariciftci, N. S.; Smilowitz, L.; Heeger, A. J.; Wudl., F. *Science* **1992**, *258*, 1474.
(9) Krishnan, R. S.; Mackay, M. E.; Duxbury, P. M.; Hawker, C. J.; Asokan, S.; Wong, M. S.; Goyette, R.; Thiyagarajan., P. *J. Phys.: Condens. Matter* **2007**, *19*, 356003.
(10) Gupta, S.; Zhang, Q.; Emrick, T.; Balazs, A. C.; Russell., T. P. *Nat. Mater.* **2006**, *5*, 229.
(11) Lee, J. Y.; Zhang, Q.; Emrick, T.; Crosby., A. J. *Macromolecules* **2006**, *39*, 7392.
(12) Ma, W.; Yang, C.; Gong, X.; Lee, K.; Heeger., A. J. *Adv. Func. Mater.* **2005**, *15*, 1617.
(13) Buxton, G. A.; Clarke., N. *Phys. Rev. B* **2006**, *74*, 085207.
(14) Campoy-Quiles, M.; Ferenczi, T.; Agostinelli, T.; Etchegoin, P. G.; Kim, Y.; Anthopoulos, T. D.; Stavrinou, P. N.; Bradley, D. D. C.; Nelson., J. *Nat. Mater.* **2008**, *7* (2), 158–164.
(15) Kiel, J. W.; Eberle, A. P. R.; Mackay., M. E. *Phys. Rev. Lett.* **2010**, *105*, 168701.
(16) Kiel, J. M.; Kirby, B. J.; Majkrzak, C. F.; Maranville, B. B.; Mackay., M. E. *Soft Matter* **2010**, *6*, 641.
(17) Wang, T.; Dunbar, A. D. F.; Staniec, P. A.; Pearson, A. J.; Hopkinson, P. E.; MacDonald, J. E.; Lilliu, S.; Pizzey, C.; Terrill, N. J.; Donald, A. M.; Ryan, A. J.; Jones, R. A. L.; Lidzey., D. G. *Soft Matter* **2010**, *6* (17), 4128–4134.
(18) Hoppe, H.; Sariciftci., N. S. *J. Mater. Chem.* **2006**, *16*, 45.
(19) Yang, X.; Loos., J. *Macromolecules* **2007**, *40*, 1353.
(20) Wong, H. C.; Cabral., J. T. *Phys. Rev. Lett.* **2010**, *105*, 038301.
(21) Wong, H. C.; Sanz, A.; Douglas, J. F.; Cabral., J. T. *J. Mol. Liq.* **2010**, *153*, 79.
(22) Gunton, J. D.; San-Miguel, M., Sahni, P. S. In *Phase Transitions and Critical Phenomena*; Domb, C., Lebowitz, J. L., Eds.; Vol 8, pp 267, Academic: New York, 1983.
(23) Sung, L.; Karim, A.; Douglas, J. F.; Han., C. C. *Phys. Rev. Lett.* **1996**, *76*, 4368.
(24) Ermi, B. D.; Karim, A.; Douglas., J. F. *J. Polym. Sci., Polym. Phys. Ed* **1998**, *36*, 191.
(25) For comparison purposes, selected wafers were Piranha-cleaned by immersing into a bath of 30/70 volume fraction of 30% H_2O_2 and 96% H_2SO_4 at 80 °C for 1 h, washed with excess deionized

water, and dried with nitrogen. All remaining experiments were carried out on as received wafers with native 2 nm oxide layer, flushed with toluene and dried with nitrogen before use.

(26) To ensure complete solvent removal and rule out nonequilibrium effects caused by spin coating, selected nanocomposite films with 5 wt % C_{60} were preannealed at 140 °C, which corresponds to the threshold agglomeration temperature T_c for 5 wt % films and is sufficiently higher than T_g. Subsequent 60 min annealing at 180 °C produced identical results to specimens prepared without preannealing/further drying.

(27) Mackay, M. E.; Tuteja, A.; Duxbury, P. M.; Hawker, C. J.; Van Horn, B.; Guan, Z. B.; Chen, G. H.; Krishnan., R. S. *Science* **2006**, *311*, 1740.

(28) Waller, J. H.; Bucknall, D. G.; Register, R. A.; Beckham, H. W.; Leisen, J.; Campbell, K. *Polymer* **2009**, *50* (17), 4199–4204.

(29) Sanz, A.; Wong, H. C.; Douglas, J. F.; , Cabral, J. T. Manuscript submitted for publication (2011).

(30) Xie, R.; Karim, A.; Douglas, J. F.; Han, C. C.; Weiss., R. A. *Phys. Rev. Lett.* **1998**, *81*, 1251.

(31) Seemann, R.; Herminghaus, S.; Jacobs., K. *Phys. Rev. Lett.* **2001**, *86* (24), 5534–5537.

(32) Brochard, F.; Daillant., J. *Can. J. Phys.* **1990**, *68*, 1084.

(33) Holmes, M. A.; Mackay, M. E.; Giunta., R. K. *J. Nanopart. Res.* **2007**, *9*, 753.

(34) Yaklin, M. A.; Duxbury, P. M.; Mackay., M. E. *Soft Matter* **2008**, *4*, 2441.

(35) Mackay, M. E.; Hong, Y.; Jeong, M.; Hong, S.; Russell, T. P.; Hawker, C. J.; Vestberg, R.; Douglas., J. F. *Langmuir* **2002**, *18*, 1877.

(36) Tseng, T. C.; McGarrity, E. S.; Kiel, J. W.; Duxbury, P. M.; Mackay, M. E.; Frischknecht, A. L.; Asokan, S.; Wong., M. S. *Soft Matter* **2010**, *6*, 1533.

(37) Doi, M. In *Theoretical challenges in the dynamics of complex fluids.*; McLeish, T. C. B., Ed.; NATO ASI Series, Series E: Applied Sciences; Kluwer Academic: Dordrecht, The Netherlands, 1997; Vol. 339, pp 293.

(38) Avrami., M. *J. Chem. Phys.* **1940**, *7*, 1103.

(39) Avrami., M. *J. Chem. Phys.* **1940**, *8*, 212.

(40) Avrami., M. *J. Chem. Phys.* **1940**, *9*, 177.

(41) Maffezzoli, A.; Kenny, J. M.; Torre., L. *Thermochim. Acta* **1995**, *269/270*, 185.

(42) Plazek., D. J. *J. Phys. Chem.* **1965**, *69*, 3480.

(43) Ngai, K. L.; Plazek, D. J. In *Physical Properties Handbook*. Ed. Mark, J. E., American Institute of Physics: Woodbury, NY, 1996.

(44) Tuteja, A.; Mackay, M. E.; Narayanan, S.; Asokan, S.; Wong., M. S. *Nano Lett.* **2007**, *7*, 1276.

(45) Wong, H. C.; Cabral, J. T. *Submitted for publication* **2011**.

(46) Narayanan, S.; Lee, D. R.; Guico, R. S.; Sinha, S. K.; Wang., J. *Phys. Rev. Lett.* **2005**, *94*, 145504.

(47) Wong, H. C.; Cabral., J. T. *J. Phys.: Conf. Ser.* **2010**, *247*, 012046.

(48) Keddie, J. L.; Jones, R. A. L.; Cory., R. A. *Europhys. Lett.* **1994**, *27*, 59.